Journal of Engineering Science and Technology
Vol. 21, No. 2 (2026) 662 - 679

BUCKLING BEHAVIOR FOR AA7075 COLUMNS UNDER CORROSION EFFECT AND VARIABLE LOAD

ALI Y. KHENYAB*, MUHANNAD Z. KHALIFA

Department of Refrigeration and Air Conditioning Engineering,
Al Salam University College, Baghdad, Iraq
*Corresponding Author: Ali.y.khenyab@alsalam.edu.iq

Abstract

This study investigates how corrosion affects the buckling response of AA7075 aluminium columns under increasing dynamic axial loads. Both long and intermediate columns were examined to assess the role of slenderness ratio in such conditions. Experimental work involved testing multiple specimens under dynamic compression, including standardized buckling tests, with comparisons made between corroded and intact samples. Lateral deformation was measured accurately using a digital dial gauge placed at 0.7 of the column length from the fixed end. The analysis relied on established models, including Euler's equation for long columns, Perry–Robertson for intermediate columns, and the Euler–Johnson approach for transitional ranges. According to design standards, lateral deflection was limited to 1% of the effective length. To replicate corrosion effects, specimens were buried for 60 days before testing. The findings indicate that corrosion reduces structural performance. After 60 days of exposure, the ultimate compressive strength decreased by 1.78% compared to uncorroded specimens. The critical buckling load also declined with increasing corrosion time, reaching a maximum reduction of 4.24%. Comparison with theoretical models showed that the Perry-Robertson equation, using a safety factor of 1.3, best matched the experimental data, while the Euler–Johnson and Euler equations were less accurate for intermediate–short and long columns, respectively. Finite element analysis in ANSYS closely matched experiments, particularly with a 1.1 safety factor. Results confirm corrosion weakens aluminium columns, while reliable models predict buckling behaviour. Additionally, AkzoNobel Intergard epoxy effectively protects AA7075 columns, preserving performance in saline environments.

Keywords: Aluminium AA7075 columns, Column constant, Deflection of column, Elastic buckling, Process of oxidation (corrosion).

1. Introduction

Buckling is a structural failure characterized by sudden lateral deformation under axial compression. Even small axial forces can trigger shape changes, and exceeding a critical load may lead to severe instability and loss of load-bearing capacity. Therefore, evaluating buckling is crucial in structural analysis [1].

Ozkan and Ozkol [2] highlighted the pronounced sensitivity of columns to axial loading, noting that even minimal forces can induce geometric changes. As the applied load nears the critical buckling threshold, nonlinear deformations become significant, necessitating the incorporation of geometric nonlinearity in advanced structural analysis and design.

Wang et al. [3] experimentally investigated local buckling in aluminium alloy I-columns using 15 stub columns and 48 tensile specimens of 6061-T6 and 6063-T5. They found low ductility in 6061-T6 and early buckling in slender plates, though post-buckling strength remained. Most design codes underestimated load capacity, except the American standard, which proved more accurate.

Chang et al. [4] studied the stability and failure strength of slender aluminium alloy columns with non-uniform cross-sections, identifying local and distortional buckling through inflection points in force–deflection curves.

Vellaichamy et al. [5] analysed the buckling behaviour of columns with varying cross-sections, focusing on critical load capacity. Using Euler's theory and ANSYS 19.2, they found that column length and cross-section influence elastic instability. Eigenvalue analysis showed less than 0.8% variation, confirming the reliability of the numerical method for regular, uniform columns.

Piluso et al. [6] examined the ultimate strength of aluminium channel sections under uniform compression, focusing on local buckling. They compared the Deformation Theory of Plasticity (DTP), which captures elastic–plastic behaviour and plate interaction, with the simplified Effective Thickness Method (ETM) based on Eurocode 9. ETM was extended to include material nonlinearity and boundary conditions. Both methods were validated through stub column tests at the University of Salerno.

Li et al. [7] assessed SHS columns of high-strength 7A04-T6 aluminium under axial and tensile loads. Validated FE models supported 480 parametric studies, showing that current design codes underestimate axial capacity by ~9%. Modified design curves and an adapted Continuous Strength Method (CSM) improved accuracy, though the Eurocode-based method fell short of safety requirements.

Liu et al. [8] examined interactive buckling in 6063-T5 aluminium square tubes under axial and eccentric compression. Testing eleven thin-walled columns and validating FE simulations, they found that greater slenderness suppresses local buckling, causing overall buckling to occur first.

The research gap of this study is that existing previous research addresses steel and other aluminium alloys like AA6061, with limited experimental validation for AA7075. There is a lack of full-scale testing on medium-to-long AA7075 columns under axial loads, particularly regarding the effects of long-term exposure (e.g., salt spray, marine environments).

The study investigates the buckling behaviour of AA7075 aluminium alloy columns under corrosion and dynamic axial loading. It examines long and intermediate columns with varying slenderness ratios exposed to natural saline corrosion for 60 days, and compares results with Euler, Perry–Robertson, and Euler–Johnson models. Lateral deflection was precisely measured, and the protective efficiency of the epoxy coating was evaluated. Findings were validated through ANSYS simulations with safety factors, providing practical recommendations for structural design in corrosive environments.

2. Buckling Critical Load Formulas

Buckling formulas calculate the maximum axial load a structural element, like a column, can bear before becoming unstable and buckling. They predict the critical load causing sudden lateral deflection and possible failure. These include [9]:

2.1. Euler formula

Euler's formula plays a fundamental role in structural mechanics and engineering by providing a theoretical basis for predicting the critical buckling load of slender columns subjected to axial compression. Figure 1 shows the support conditions of the column. Euler's stability analysis focuses on a column with fixed-pinned end conditions, representing a fundamental example of his method [10]. It is essential in column analysis and design, as it defines the maximum compressive force a column can bear before losing stability [9]. Euler's famous Eq. (1) characterizes the behaviour of slender, idealized columns under axial compression, predicting their tendency for small elastic bending [9]. Its scientific significance includes:

- Predicting the critical buckling load
- Linking material and geometric properties
- Incorporating boundary conditions
- Serving as a foundation for advanced theories
- Enabling wide engineering applications
- Enhancing structural safety

$$P_{cr} = \frac{\mu^2.E.I}{K^2L^2} \quad (1)$$

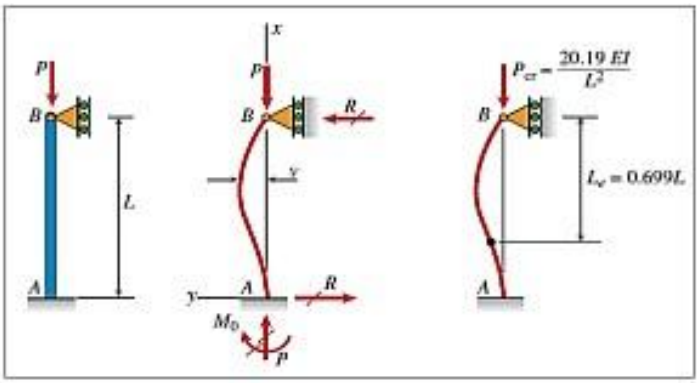

Fig. 1. Condition of column (fixed pinned) [10].

2.2. Perry-Robertson formula

To address the limitations of the Johnson and Euler formulas, applicable mainly to intermediate and slender columns, respectively, the Perry–Robertson model was developed as a more adaptable approach [11]. It accounts for initial curvature, eccentric loading, and material imperfections, offering a realistic prediction of compressive behaviour. By incorporating these real-world factors, the semi-empirical model improves the accuracy of critical buckling load estimates, as expressed in Eq. (2) [12].

$$P_{cr} = \frac{N_E}{1+\alpha\frac{e_0}{r}.\frac{N_E}{A.\sigma_y}} \tag{2}$$

2.3. Euler–Johnson formula

The Euler formula is valid only for long columns with a slenderness ratio exceeding a specific column constant (Cc). Aside from incorporating the modulus of elasticity, it does not consider other material properties [13]. Since the slenderness ratio depends solely on column dimensions, the Euler equation estimates the critical load PcrP_{cr}Pcr based on geometry rather than strength. In contrast, the Johnson formula applies to short or intermediate columns with lower slenderness ratios, where failure is due to material yielding under higher stress. This relationship is captured in Eq. (3) [10].

The Euler–Johnson formula plays a key role in science and engineering by linking geometric and material factors in column stability analysis. It is also valuable in solving mathematical problems, particularly those involving differential equations and structural mechanics.

$$P_{cr} = \frac{A.\sigma_y}{1+\alpha\left(\frac{K.L}{r}\right)^2} \tag{3}$$

2.4. The Slenderness ratio (S.R)

The slenderness ratio (S.R.) is defined as the effective column length divided by its least radius of gyration, as presented in Eq. (4) [14]. Table 1 presents the corresponding lengths of the columns [14].

$$\mathrm{S.R}(\lambda) = \frac{\mathrm{kL}}{\mathrm{r}} \tag{4}$$

The Column constant (Cc).

$$\mathrm{Cc} = \sqrt{\frac{2\pi^2\mathrm{E}}{\sigma_\mathrm{y}}} \tag{5}$$

Table 1. Column types based on slenderness ratio [14].

Column Type	Slenderness Ratio	Behaviour under Buckling
Short Column	$\lambda < 50$	Fails by crushing, not buckling
Medium Column	$50 \leq \lambda \leq 100–120$	Fails by combined crushing. and buckling
Long Column	$\lambda > 100–120$	Fails primarily by buckling

In structural engineering, column buckling is largely affected by end conditions, which define effective length and load capacity. The main types are [12]:

- Fixed–Free (Fig. 2 (a)): One end fixed, one free; weakest resistance; effective length = 2× actual length.
- Pinned–Pinned (Fig. 2 (b)): Ends can rotate but not translate; moderate resistance.
- Fixed Pinned (Fig. 2 (c)): One end fixed, one pinned; intermediate resistance; effective length ≈ 0.7× actual length.
- Fixed–Fixed (Fig. 2 (d)): Both ends restrained; strongest resistance; effective length = 0.5× actual length.

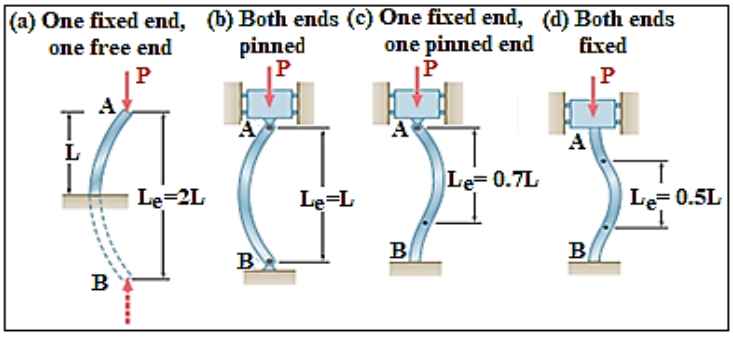

Fig. 2. End fixity type [12].

3. Chemical Composition

The chemical test results from the Organization for Industrial Restoration and Inspection are presented in Table 2. The results are compared with the U.S. standard [15].

Table 2. Standard and experimental chemical constituents of AA7075, [15].

Material	Si%	Fe%	Cu %	Mn%	Mg %	Cr %	Zn %	Ti%	Al %
Standard	0.4	0.5	1.2-2.0	0.30	2.1-2.9	0.18-0.28	5.1-6.1	0.20	Balance
Experimental	0.36	0.46	1.9	0.25	2.65	o.21	5.7	0.17	Balance

4. Experimental Work

AA7075 aluminium alloy was chosen for use in this study due to its favourable mechanical properties. The detailed chemical composition of the alloy is presented in Table 2. Table 3 summarizes standard and experimentally determined mechanical properties for a comprehensive comparison. Table 4 details the dimensional specifications of rigid test specimens made from 7075 aluminium alloy, ensuring accurate property evaluation and consistent procedures.

Table 3. Mechanical properties of standard and experimental AA7075 [15].

Property	σ_u (MPa)	σ_y (MPa)	E (GPa)	μ	G (GPa)	HB
Standard [11]	228	103	71.7	0.3	72	26
Experimental	228	111	72	0.3	72	26

Figure 3 shows structural specimens prepared in two conditions: pre-induced corrosion and corrosion-free, enabling analysis of corrosion effects on stability and compressive load capacity. All equipment calibrations were performed at the General Company for Engineering Inspection and Qualification under the Ministry of Industry and Minerals [15].

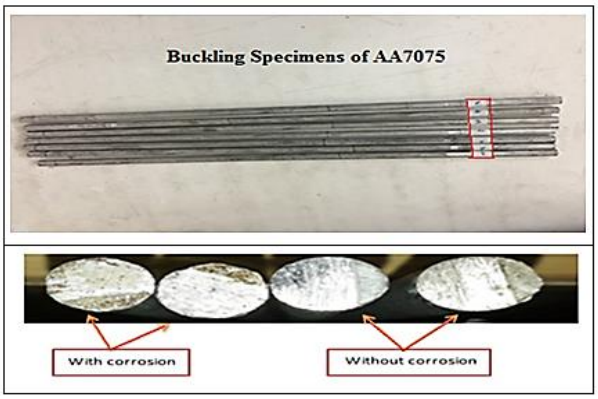

Fig. 3. Buckling specimens with and without corrosion.

Table 4. Provides the rigid specimen's measurements for the aluminium AA7075 alloy.

Sp. No.	L mm	Le mm	D mm	R mm	I mm^4	A mm^2	SR	Cc	Type of column
1	300	210	8	2	201.06	50.26	105	105	long
2	400	280	6	1.5	63.61	28.27	186.66	105	long
3	300	210	6	1.5	63.61	28.27	140	105	long
4	300	210	10	2.5	490.87	78.53	84	105	intermediate
5	200	140	10	2.5	490.87	78.53	56	105	intermediate
6	200	140	6	1.5	63.61	28.27	93.33	105	intermediate

4.1. Buckling test

Specimens made of AA7075 aluminium alloy were tested using a rig machine, as illustrated in Fig. 4. The ends of the test columns were supported by fixed pins capable of rotating at a speed of 17 revolutions per minute (rpm). The testing rig is equipped with an integrated system that enables the application of both torsional and compressive loads, allowing for a comprehensive evaluation of the material's mechanical response under combined loading conditions. To enhance measurement precision, the deformation of the column is recorded using a laser sensor system equipped with an audible alert, mounted on a digital calliper with a precision of 0.01 mm, along with a mechanical dial indicator placed at the centre of the specimen. Figure 4 shows that a dedicated experimental setup, commonly referred to as a buckling test rig, was utilized to simulate and analyse the structural instability phenomena that occur in slender components subjected to axial compressive loads. This apparatus is specifically designed to replicate real-world buckling conditions under controlled laboratory environments, allowing for accurate measurement and observation of critical thresholds.

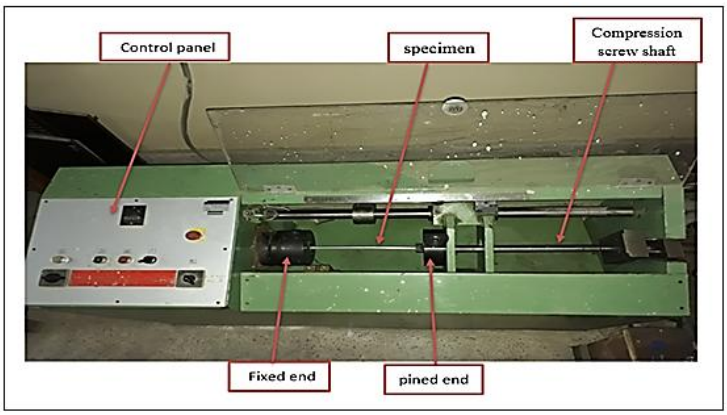

Fig. 4. Buckling test rig.

The permitted lateral deformation of the specimen is 1% of its length. When the axial force is removed, the column returns to its starting point after the specimen's lateral deflection reaches this percent and stays below it. This is referred to as the columns' critical buckling. The sample fails when the lateral deflection is greater than this ratio [15].

4.2. Specimen test

Figures 5(a) and (b) depict the two primary categories of buckling specimens employed in the present investigation. These categories were established to enable a comparative analysis between undamaged and environmentally deteriorated structural elements. The first category, Fig. 5(a), is composed of intact, non-corroded specimens. These samples were preserved in their original condition and were used as a baseline or control group to assess the standard buckling behaviour without any external degradation factors.

In contrast, the second category, Fig. 5(b), includes specimens that underwent an artificial corrosion process. These samples were buried in soil for a continuous duration of 60 days. This exposure aimed to replicate the effects of environmental conditions that typically contribute to the deterioration of structural materials over time. Once the corrosion phase was completed, the deteriorated samples underwent buckling examinations, as illustrated in Fig. 6, during which the axial load was incrementally applied. This testing aimed to assess the structural integrity and failure characteristics of the corroded specimens when subjected to gradually increasing compressive forces.

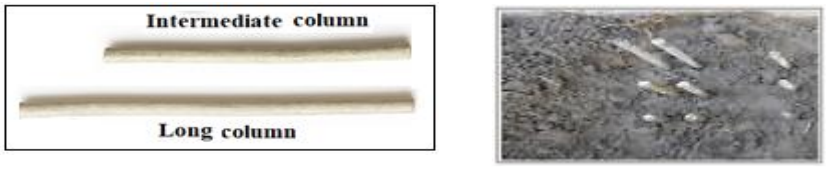

(a) The first category **(b) the second category**

Fig. 5. Specimens of AA7075.

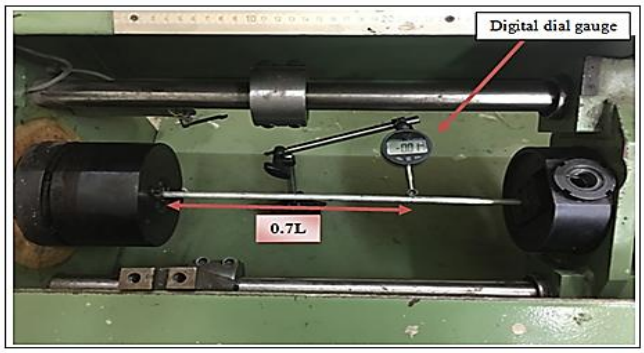

Fig. 6. Buckling specimen during the test with digital Dial gauge.

4.3. Buckling test rig

The buckling test rig incorporates essential components for precise mechanical testing, utilizing hydraulic or mechanical actuators to apply compressive loads. It supports both displacement-controlled and force-controlled modes, with load capacities ranging from a few kilonewtons to several meganewtons, depending on the rig configuration and specimen design. Adjustable fixtures are employed to replicate various boundary conditions, such as pinned, fixed, free, or guided ends, ensuring proper specimen restraint. Accurate alignment is crucial to prevent eccentric loading and to guarantee reliable test results. Measurement systems play a critical role in capturing the specimen's response during testing. Load cells accurately measure applied forces, while LVDTs record axial shortening and lateral deflection. Strain gauges monitor strain distribution, and optical devices or cameras are often used to document deformation and visualize buckling behaviour. The rig's steel frame is engineered for high rigidity to minimize deformation under load, ensuring stable and repeatable testing conditions. A computer-controlled system manages the application of load or displacement and captures real-time data, with an automatic shutdown function activated at the critical buckling point. For operator safety, the rig is equipped with safety features such as emergency stop controls and protective guards, which help mitigate risks associated with sudden specimen failure or collapse.

4.4. Effect of corrosion duration on the critical strength of column AA7075 and its development

This study explores the impact of soil salinity-induced corrosion on the critical buckling capacity of AA7075 columns. Corrosion was experimentally induced by immersing the specimens in a highly concentrated saline solution, selected to replicate salinity levels commonly observed in saline soils (Table 5 [16]). A total of twenty columns were subjected to corrosion for varying durations, with exposure intervals increasing in three-day increments, while one column was preserved as a non-corroded control specimen.

To evaluate the effectiveness of protective measures, an epoxy coating was applied using AkzoNobel Intergard epoxy at a thickness of 350 μm to mitigate the detrimental effects of corrosion and further examine the relationship between

critical strength and corrosion exposure time. The coating procedure was conducted in the laboratories of the Ministry of Science and Technology.

Table 5. The composition of a saline solution with a concentration that closely matches the levels typically found in saline soils [16].

Soil Salinity Class	ECe (dS/m)	Approx. Salt Content (% by weight)
Non-saline	< 2	< 0.15 %
Slightly saline	2 – 4	0.15 – 0.30 %
Moderately saline	4 – 8	0.30 – 0.60 %
Strongly saline	8 – 16	0.60 – 1.20 %
Very strongly saline	> 16	> 1.20 %

5. Results and Discussion

5.1. Results of tensile tests

Tensile testing was conducted, and the experimental results are summarized in Table 6. The mechanical performance of the AA7075 aluminium alloy was evaluated under two conditions: in its original state and after 60 days. The results showed a slight reduction in both ultimate tensile strength (σ_u) and yield strength (σ_γ), while the elastic modulus (E) and shear modulus (G) remained nearly unchanged.

Specifically, the ultimate tensile strength decreased from 228 MPa to 224 MPa after 60 days, representing a reduction of approximately 1.75%. Similarly, the yield strength declined from 111 MPa to 106 MPa, indicating a decrease of about 4.5%. These moderate reductions suggest a slight loss in the alloy's resistance to deformation and failure under mechanical loading, potentially attributed to microstructural aging phenomena such as dislocation rearrangement or minor precipitate coarsening during storage.

In contrast, the elastic modules showed a negligible change, decreasing from 72 × 10^3 MPa to 71 × 10^3 MPa, while the shear modulus dropped slightly from 26 × 10^3 MPa to 25 × 10^3 MPa. These minimal variations imply a marginal decrease in the alloy's stiffness over the 60 days.

These findings agree with previous studies on AA7075 aluminium alloys, showing typical behaviour under natural aging or mild environmental exposure. Similar strength reductions were reported by [11] and [12], especially in T6 and T73 tempers, due to aging-related microstructural changes. The slight strength loss observed here is consistent with AA7075's sensitivity to time-dependent softening, though less severe, likely due to shorter exposure time and absence of harsh corrosion. Additionally, the minimal changes in elastic and shear moduli support earlier data, which show stiffness is generally unaffected by aging unless major microcracking occurs. Overall, the results confirm that moderate aging slightly reduces strength, while stiffness remains stable in the short term.

Table 6. Tensile testing was performed on both rusted and non-corroded AA7075 samples.

AA7075	σ_u (MPa)	σ_y (MPa)	E X10^3 (MPa)	G X10^3 (MPa)
AS received	228	111	72	26
60 days	224	106	71	25

5.2. Buckling test results

To test the specimens under increasing loads, columns were fabricated with varying slenderness ratios. The dynamic buckling test results for AA7075 column samples, both uncorroded (AS received) and corroded (Group 2), are presented in Table 7. To maintain structural integrity during buckling, the damaged surface of each corroded column must be constrained. As the corrosion duration increases, the buckling life (in cycles) of the pre-corroded samples decreases compared to the uncorroded ones, leading to a reduction in critical buckling load. A comparison between the corroded specimens (Group 2) and the uncorroded specimens (Group 1) indicates that dynamic buckling strength significantly decreases as a function of corrosion after 60 days of exposure. The relationship between corrosion duration and the column's critical buckling load is developed through controlled experimental testing combined with empirical modelling techniques, primarily regression analysis. The values of Table 6 change are discussed as follows: specimen 1 (Long Column), before corrosion: 2260 N, after 60-day corrosion: 2212 N, load decrease: 2.12%, observation: small reduction in load capacity, initial and critical deformations remain unchanged. Specimen 2 (Long Column), moderate reduction in buckling load; very slight increase in initial deformation (1.3 mm to 1.31 mm), specimen 3 (Long Column), Similar pattern to specimen 2. Load decreased, deformation values stayed constant, specimen 4 (Intermediate Column), before corrosion: 8478 N, after corrosion: 8316 N, load decrease**:** 1.91%, and observation: minor effect of corrosion. The deformation is almost identical before and after corrosion. From Table 6 shows, corrosion leads to a slight to moderate decrease in the critical buckling load (between 1.38% and 4.25%), deformation values (δ_{IN} and δ_{cr}) remain almost constant, showing that geometry and flexibility weren't significantly affected, long columns tend to show a slightly higher percentage reduction in buckling load compared to intermediate ones and the highest reduction was observed in specimen 2 (4.25%), while the least reduction was in specimen 6 (1.38%).

Table 7. Relationship between corrosion and buckling for lengthy and intermediary columns that are pinned or fixed.

Sp. No	AS obtained (Group 1)			60-day Corrosion (Group 2)			A decrease in the percentage of critical buckling load	Columns style
	P_{cr} (N)	δ_{IN} mm	δ_{cr} mm	P_{cr} (N)	δ_{IN} mm	δ_{cr} mm	60 days	
1	2260	0.5	3.6	2212	0.51	3.6	2.12	**Long**
2	494	1.3	4.2	473	1.31	4.2	4.25	**Long**
3	812	0.7	3.7	779	0.7	3.7	4.06	**Long**
4	8478	0.5	2.6	8316	0.5	2.62	1.91	**Intermediate**
5	3532	0.3	2.3	3413	0.3	2.3	3.37	**Intermediate**
6	1659	0.6	2.4	1636	0.6	2.4	1.38	**Intermediate**

These results are consistent with the findings reported in [17, 18]. Figure 7 presents a bar chart illustrating the effect of slenderness ratio (SR) on the critical load (Pcr) of metallic samples under two conditions: as-received (blue) and after 60 days of corrosion exposure (red), for SR values of 105, 140, and 186. At SR = 105, P_{cr} decreases from ~2200 N to ~2000 N (9.1% reduction), indicating moderate corrosion resistance. For SR = 186, Pcr drops from ~600 N to ~500 N (16.7%

reduction), showing increased sensitivity to corrosion. At SR = 140, the decrease is minimal, from ~850 N to ~800 N (5.9%), suggesting higher resilience. Overall, corrosion reduces critical load, but its impact—both absolute and relative—varies with SR. Higher SRs exhibit greater percentage loss, emphasizing the role of geometry in structural vulnerability. These findings underscore the need to consider both geometric and environmental factors in durability assessments, particularly in corrosive conditions.

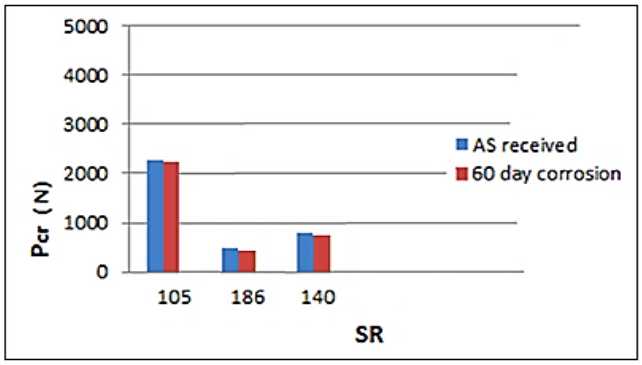

Fig. 7. The connection between corrosion and buckling for lengthy columns.

Figure 8 displays a bar chart depicting the relationship between slenderness ratio (SR) and critical load (Pcr) for metallic samples under two conditions: as-received (blue) and after 60 days of corrosion exposure (red), at SR values of 56, 84, and 93. At SR = 84, Pcr declined slightly from ~8500 N to ~8300 N (2.35%), indicating good corrosion resistance. At SR = 56, the same absolute reduction (200 N) resulted in a 5% decrease, reflecting greater relative impact. At SR = 93, the drop from ~1800 N to ~1600 N equates to an 11.11% loss, highlighting increased vulnerability in lower-strength samples. Although the absolute reduction in Pcr remains constant (~200 N), the relative impact increases as initial strength decreases. This emphasizes the importance of evaluating percentage change alongside absolute values. These findings underscore the influence of SR on structural degradation under corrosive conditions. As SR increases, corrosion sensitivity varies, indicating the need to consider both geometric and environmental factors when assessing the long-term performance of metallic structures.

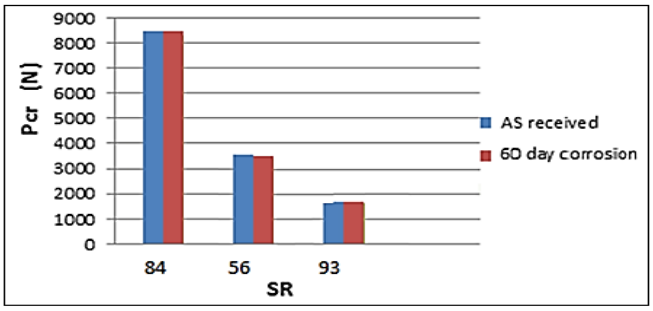

Fig. 8. The connection between corrosion and buckling for transitional columns.

5.3. Perry- Robertson formula application

The Perry-Robertson (PR) prediction of P_{cr} is not adequate when comparing the experimentally determined critical load value with the Perry-Robertson finding; nevertheless, a factor of safety of 1.3 provided a safe calculation using P_{cr} in an evolving condition. Refer to Table 8.

Table 8. Comparison between experimentally determined critical load value for intermediate and long columns with Perry-Robertson results.

Sp. No.	P_{cr} Exp. (N)		P_{cr} (Perry-Robertson) (N)		P_{cr} (Perry-Robertson) (N) With S.F of 1.3		Type of column
	AS received	60 days	AS received	60 days	AS Received	60 Days	
1	494	481	492	469	378	361	Long
2	2235	2190	2625	2515	2019	1934	Long
3	847	824	858	822	660	632	Long
4	8478	8311	9638	9281	7414	7139	Intermediate
5	4532	4420	5025	4821	3865	3708	Intermediate
6	1695	1639	1821	1745	1401	1342	Intermediate

The column may become longer if the S.R. is higher than 105. A value of 51 MPa might restrict the type of column; columns that are larger than this number are considered to belong, while columns that are less than this amount are referred to as intermediate columns. Figure 9 compares the experimental result of AA7075 with one of the ends having a strength of yield of 111 MPa, one fixed (K = 0.7) and another pinned, with the relationship between stresses at failure and ratio of slenderness as described by the Perry-Robertson equation for long and intermediary columns.

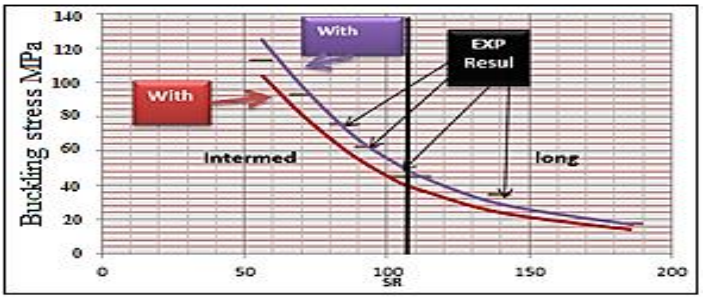

Fig. 9. AA 7075 aluminium alloy's test outcomes and the Perry-Robertson curves.

5.4. Utilizing the Johnson and Euler formulas to analyses the experimental data

During the initial design phase, Euler's and Johnson's theories help estimate critical buckling stress. In this study, Johnson's equation is applied to intermediate-length columns, while Euler's applies to long ones. For AA7075 alloy with a yield stress of 111 MPa, the transition slenderness ratio between elastic and inelastic buckling is 105, and intermediate columns begin at a ratio of 56. Although both tested cases

qualify as long columns under Euler's criteria, they also fall within Johnson's applicable range. Johnson's equation predicts a lower critical stress than Euler's for the specimens examined.

The safety factor (FoS) of 1.1 to 1.3 used in buckling calculations (as opposed to general deflection) for columns is due to the specific nature of buckling failure. This relatively small safety factor is used because buckling is governed by Euler's critical load formula, which is derived from a well-understood, idealized elastic theory. These theoretical models (e.g., Euler's formula) can predict failure loads quite accurately when the geometry and material properties are well controlled. This paper compares Euler, Johnson, and Perry-Robertson models to estimate values of the threshold load. The real practical threshold has a higher safety factor than the above formulations. The Perry–Robertson is the critical load prediction formula for long and intermediate columns, demonstrating safe estimation for corroded specimens. The safety factor ranges from 1.33 to 1.57.

Table 9 indicates that both Johnson and Euler formulas yield higher safety factors. It presents the critical loads experimentally measured and theoretically estimated using Euler-Johnson and Euler (with a 1.5 safety factor) for each specimen. Columns are classified as "Long" or "Intermediate" based on their slenderness ratio, which affects buckling behaviour. Experimental loads reflect failure points, while theoretical values include safety margins. For instance, specimen 1 (long) decreased from 494 N to 481 N over 60 days, whereas theoretical loads remained higher. Specimen 4 (intermediate) began at 8478 N, with only a slight reduction. Theoretical values consistently exceeded experimental ones, highlighting conservative design. The findings underscore the roles of column type, duration, and calculation method in determining load capacity, which is vital for structural safety.

Table 9. Comparison of the experimentally determined critical load value for intermediary and lengthy columns with the Euler-Johnson calculations.

p. No.	P_{cr} Exp. (N)		P_{cr} Euler-Johnson (N)		P_{cr} Euler with S.F (N) of 1.5		Type of column
	AS received	60 days	AS received	60 days	AS Received	60 days	
1	494	481	568	539	378	359	Long
2	2235	2190	3194	3058	2129	2038	Long
3	847	824	1010	958	673	638	Long
4	8478	8311	9750	9358	6500	6238	Intermediate
5	4532	4420	5538	5311	3692	3540	Intermediate
6	1695	1639	1636	2261	2160	1507	Intermediate

Figure 10 shows the relationship between slenderness ratio (SR) and critical buckling stress for an AA7075 aluminium column (σ_y = 127 MPa), assuming a fixed–pinned end condition (K = 0). The curve, based on Euler's and Johnson's formulas, distinguishes elastic buckling at high SR (Euler region) from inelastic buckling at low SR (Johnson region). Experimental results also reveal strain-rate sensitivity in AA7075, with increased loading rates enhancing toughness and delaying buckling onset.

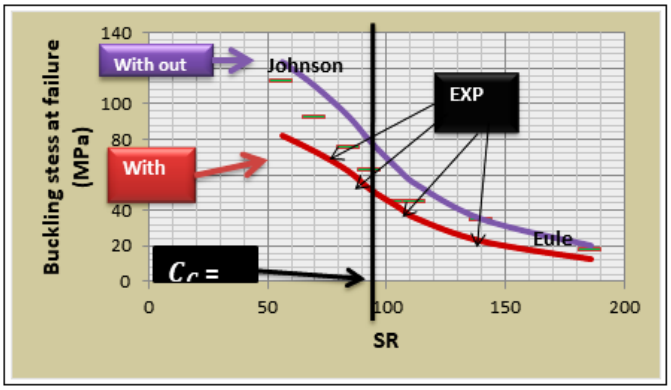

Fig. 10 Johnson-Euler curve for AA7075 aluminium alloy based on experimental findings.

5.5. Analytical ANSYS and experimental methods are compared.

Data obtained from experimental work helps ANSYS predict where and when alloys will fail under complex loads. The ANSYS package created a numerical model, and the outcomes were compared to the experimental findings. The percentage variations in the experimental and analytical findings for S.F = 1.1 are shown in Table 10. The ANSYS package17's assumption, the challenges of controlling measurements in the experimental work, and the possibility of inaccuracy when reading the experimental data are a few potential reasons for the disparities. A buckling study predicts the maximum load that a structure can support before becoming unstable or collapsing. The analysis can be carried out as a linearized buckling or a massive deformation analysis, with or without traversing unique points (buckling). For theoretical analysis, the ANSYS program was adopted.

Table 10. Comparison of the experimentally determined critical load value for intermediary and long columns with the outcomes of ANSYS.

Sp No.	P_{cr} Exp. (N)		P_{cr} ANSYS (N)		P_{cr} Euler with S.F (N) of 1.1		Column kind
	AS received	60 days	AS received	60 days	AS Received	60 days	
1	494	481	520	496	472	450	Long
2	2235	2190	2243	2109	2039	1917	Long
3	847	824	895	853	813	775	Long
4	8478	8311	9052	8317	8229	7560	Intermediate
5	4532	4420	4884	4822	4438	4383	Intermediate
6	1695	1639	1778	1691	1616	1537	**Intermediate**

Table 11 presents a comparison of the critical load (P_{cr}) predictions obtained using the Perry-Robertson formula, the Euler-Johnson approach, and ANSYS simulations. For long specimens, the Euler-Johnson method generally yields higher P_{cr} values, which can be attributed to its reliance on idealized assumptions about column behaviour. In contrast, the Perry-Robertson method and ANSYS results are more aligned in magnitude and tend to provide slightly more conservative estimates. For intermediate-length specimens, the predictions from Perry-

Robertson and Euler-Johnson are nearly identical, whereas ANSYS occasionally produces lower values, possibly due to its ability to incorporate non-ideal factors such as geometric imperfections and boundary conditions.

Table 11. Compares three methods for determining the critical buckling load (P_{cr}) in AS and after 60 days.

Sp. No.	Type	P_{cr} Perry - Robertson (N)	P_{cr} Euler-Johnson (N)	P_{cr} ANSYS (N)
		AsRec / 60days	AsRec / 60days	AsRec / 60days
1	Long	492 / 469	568 / 539	520 / 496
2	Long	2625 / 2515	3194 / 3058	2243 / 2109
3	Long	858 / 822	1010 / 958	895 / 853
4	Intermediate	9638 / 9281	9750 / 9358	9052 / 8317
5	Intermediate	5025 / 4821	5538 / 5311	4884 / 4822
6	Intermediate	1821 / 1745	1636 / 2261	1778 / 1691

This study examines how Corrosion reduces critical loads by decreasing cross-sectional area and stiffness, effects not fully addressed by Euler's theory. Numerical models incorporating corrosion-induced imperfections match experiments more closely, revealing earlier instability and mode changes. Discrepancies stem from corrosion variability and model limitations. Compared to previous work, this study uniquely emphasizes the combined impact of corrosion and variable loading, highlighting the need for improved predictive models.

5.6. Comparison of corrosion exposure duration and critical buckling strength of AA7075 columns under uncoated and coated conditions

Table 12 presents the variation in the critical buckling load of AA7075 aluminium alloy columns over 60 days, comparing untreated specimens with those coated with AkzoNobel Intergard epoxy. The second column, representing the square root of normalized time, provides a convenient non-dimensional scale to monitor the progression of exposure.

For untreated columns, the data show a gradual but consistent decrease in critical buckling load, from 494 N on day 0 to 481 N on day 60. This reduction reflects cumulative weakening likely caused by salt-induced corrosion or environmental degradation. Early in the exposure period, the decrease is minor, indicating that the material retains most of its initial load-bearing capacity. Over time, however, the decline becomes more pronounced, highlighting the progressive impact of corrosion on structural stability.

In contrast, columns treated with AkzoNobel Intergard epoxy maintain remarkable stability throughout the same period. Starting at 494 N, the critical load remains nearly constant, decreasing only slightly to 491.87 N by day 60. This demonstrates that the epoxy effectively protects the alloy from environmental effects, preserving its buckling performance.

The comparison clearly shows the protective benefit of the epoxy coating. Untreated specimens experience a cumulative reduction of approximately 13 N (around 2.6%) over 60 days, while coated specimens show a minimal reduction of about 2 N (less than 0.5%). Therefore, applying an appropriate protective coating

can significantly enhance the durability and long-term structural performance of AA7075 columns in corrosive environments.

Table 12. Comparison of corrosion exposure duration and critical buckling strength of AA7075 Columns with and without AkzoNobel Intergard epoxy coating.

Day	√ (t/tmax)	critical buckling load (N)	
		Without treatment	Coating with AkzoNobel Intergard epoxy
0	0.0000	494.00	494.00
3	0.2236	491.91	493.99
6	0.3162	491.06	493.99
9	0.3873	490.38	493.99
12	0.4472	489.77	493.99
15	0.5000	489.29	493.96
18	0.5477	488.86	493.93
21	0.5916	488.47	493.93
24	0.6325	488.10	493.91
27	0.6710	487.75	493.90
30	0.7071	487.42	493.90
33	0.7416	487.11	493.90
36	0.7746	486.82	493.90
39	0.8062	486.54	493.87
42	0.8367	486.27	493.66
45	0.8660	486.01	493.45
48	0.8944	485.76	493.20
51	0.9219	485.52	493.01
54	0.9487	485.29	492.91
57	0.9747	485.06	492.77
60	1.0000	481.00	491.87

6. Conclusions

The influence of corrosion duration on the buckling behaviour of AA7075 columns was investigated. The study yielded the following findings:

- Extended corrosion exposure results in a decline in mechanical properties. Specifically, specimens subjected to 60 days of corrosion exhibited an approximately 1.78% reduction in ultimate strength compared to uncorroded specimens
- Corrosion time also decreases the critical buckling load. For example, intermediate columns showed a 4.2% reduction, while long columns experienced a 2.6% reduction after prolonged corrosion exposure.
- The experimental data aligned well with predictions made using the Perry–Robertson formula when a safety factor of 1.3 was applied, leading to improved agreement.
- In contrast, the Johnson equation for short and intermediate columns and the Euler equation for long columns did not produce results that satisfactorily matched the experimental data regarding critical buckling.
- ANSYS simulations closely matched experimental and analytical results with a 1.1 safety factor, confirming model accuracy near the buckling limit. While

offering detailed insights, their reliability depends on model quality, typically aligning with analytical and experimental outcomes.

- The findings demonstrate that applying an epoxy coating significantly mitigates the loss of critical buckling strength in AA7075 columns exposed to corrosive environments, reducing the strength degradation from approximately 2.6% in uncoated samples to less than 0.5% in coated ones.

Suggestions for Research Development

AA7075 is a high strength aluminium alloy commonly used in aerospace, marine, and defence applications. The following suggestions aim to advance research in experimental, computational, and practical fields.

- Examine whether buckling resistance exhibits an initial sharp decline or follows a threshold-driven degradation pattern.
- Explore the interaction between corrosion-induced wall thinning and localized stress concentration zones.
- Implement multi-factor controlled environmental chamber testing to simulate complex service conditions.
- Using a coating method that uses an 80-100 μm epoxy base and a 40-60 μm polyurethane topcoat, for a total of 120-160 μm [~~20~~ 19] to increase the protection of the columns from corrosion due to soil salinity.

Nomenclatures

A	Cross-sectional area, m^2
E	Elastic modulus, N/m^2.
e_0	Initial eccentricity of the load, mm
f_y	Yield strength of the material
I	Inertia moment, m^4
K	Effective length factor (dimensionless), Unitless.
L	overall length of the columns, m
N_E	Euler's elastic buckling load, N.
P_{cr}	Critical axial load causing buckling, N
r	Radius of gyration of the column cross-section, m.
Greek Symbols	
α	Perry-Robertson imperfection factor (usually 0.5 to 0.8)
λ	Slenderness Ratio
σ_y	yield stress, N/m^2

References

1. Bhoi, R.M.; and Kalurkar, L.G. (2014). Study of the buckling behaviour of beams and columns. *IOSR Journal of Mechanical and Civil Engineering* (*IOSR-JMCE*), 11(4), 36-48.
2. Ozkan, A.; and Ozkol, I. (2014). Buckling analysis of inclined beam-column structures by using differential transform method (DTM). *Applied Mechanics and Materials*, 390, 251-265.

3. Wang, Y.; Chang T.; Shi, Y.; and Yuan H. (2015). Experimental study on local buckling behaviour of aluminum alloy columns under uniform compression. *Journal of Building Structure*, 36(5), 46-43.
4. Chang Y.; Liu, M.; and Wang, P. (2016). Interacted buckling failure of thin-walled irregular-shaped aluminium alloy column under axial compression. *Thin-Walled Structures*, 107, 627-647.
5. Vellaichamy, P.; Kumarasamy K.; Navaneetha, S.; and Senthilkumar, V. (2019). Buckling analysis of columns. *Journal of Engineering (IOSR JEN)*, 10-17.
6. Piluso, V.; Pisapia, A.; and Rizzano, G. (2022). Local buckling of aluminium channels under uniform compression: Theoretical analysis and experimental tests. *Thin-Walled Structures*, 179, 109511.
7. Li, B. et al. (2022). Flexural buckling of extruded high-strength aluminium alloy SHS columns. *Thin-Walled Structures*, 179, 109717.
8. Liu, X.C.; Wang S.P.; Chen, X.; and Jia, S.Z. (2025). Experimental study and design method of interactive buckling of 6063-T5 aluminum alloy square tube under axial and eccentric compression. *Thin-Walled Structures*, 210, 112976.
9. Chen, J.-K.; and Li, L.-Y. (2013). Elastic axially compressed buckling of battened columns. *International Journal of Mechanical Sciences*, 77, 1-7.
10. Avcar, M. (2014). Elastic buckling of steel columns under axial compression. *American Journal of Civil Engineering*, 2(3), 102-108.
11. Li B. et al. (2022). Flexural buckling of extruded high-strength aluminium alloy SHS columns. *Thin-Walled Structures*, 179, 109717.
12. Muvdi, B.; and Elhouar, S. (2016). *Mechanics of Materials*. CRC Press.
13. Li B.; He P.; Wang J.; and Wang Y. (2024). Behaviour and design of extruded high-strength aluminium alloy SHS beam columns. *Sustainable Structures*, 4(3), 000059.
14. You X. et al. (2024). A review of research on aluminium alloy materials in structural engineering. *Developments in the Built Environment*, 17, 100319.
15. Ozer G.; and Karaaslan A. (2017). Properties of AA7075 aluminium alloy in aging and retrogression and reaging process. *Transactions of Nonferrous Metals Society of China*, 27(11), 2357-2362.
16. Lan, T. et al. (2023). Identification of saline soils using soil geochemical data: a case study in soda-salinization areas, NE China. *Sustainability*, 15(12), 9302.
17. Bader, A.M.; Alazawi, D.A.; Al_Alkawi, H.J.M.; and Faris, S.T. (2022). Effect of shot peening on the critical buckling load of stainless steel 304 columns immersed in seawater. *Curved and Layered Structures*, 9(1), 442-450.
18. Soltani, M.; Soltani, A.; and Civalek, O. (2022). Interaction of the lateral buckling strength with the axial load for FG micro-sized I-section beam–columns. *Thin-Walled Structures*, 179, 121-133.
19. Xue, Q.; Xu, S.; Li, A.; and Wang, Y. (2024). Local–overall buckling behaviour of corroded intermediate compression-bending H-section steel columns. *Engineering Structures*, 308, 118025.